

MEASUREMENT AND MODELING OF BED SHEAR STRESS UNDER SOLITARY WAVES

Jaya Kumar Seelam¹, Paul A. Guard² and Tom E. Baldock³

Abstract: Direct measurements of bed shear stresses (using a shear cell apparatus) generated by non-breaking solitary waves are presented. The measurements were carried out over a smooth bed in laminar and transitional flow regimes ($\sim 10^4 < Re < \sim 10^5$). Measurements were carried out where the wave height to water depth (h/d) ratio varied between 0.12 and 0.68; maximum near bed velocity varied between 0.16m/s and 0.51m/s and the maximum total shear stress (sum of skin shear stress and Froude-Krylov force) varied between 0.386Pa and 2.06Pa. The total stress is important in determining the stability of submarine sediment and in sheet flow regimes. Analytical modeling was carried out to predict total and skin shear stresses using convolution integration methods forced with the free stream velocity and incorporating a range of eddy viscosity models. Wave friction factors were estimated from skin shear stress at different instances over the wave (viz., time of maximum positive total shear stress, maximum skin shear stress and at the time of maximum velocity) using both the maximum velocity and the instantaneous velocity at that phase of the wave cycle. Similarly, force coefficients obtained from total stress were estimated at time of maximum positive and negative total stress and at maximum velocity. Maximum positive total shear stress was approximately 1.5 times larger than minimum negative total stress. Modeled and measured positive bed shear stresses are well correlated using the best convolution model, but the model underestimates the data by about 4%. Friction factors are dependent on the choice of normalizing using the maximum velocity, as is conventional, or the instantaneous velocity. These differ because the stress is not in phase with the velocity in general. Friction factors are consistent with previous data for monochromatic waves, and vary inversely with the square-root of the Reynolds number. The total shear stress leads the free stream fluid velocity by approximately 50° , whereas the skin friction shear stress leads by about 30° , which is similar to that reported by earlier researchers.

Keywords: *tsunami; bed shear stress; shear plate; friction factors; convolution integrals; solitary wave;*

¹School of Civil Engineering, The University of Queensland, Brisbane, QLD 4072, Australia, Email: j.seelam@uqconnect.edu.au; Scientist, Ocean Engineering, National Institute of Oceanography (CSIR), Dona Paula, Goa 403 004, India, Email: jay@nio.org

²BMT-WBM Pty Ltd., Brisbane, Australia, Email: paul.guard@bmtwbm.com.au

³School of Civil Engineering, The University of Queensland, Brisbane, QLD 4072, Australia, Email: t.baldock@uq.edu.au

1. INTRODUCTION

Bed shear stress is an important parameter in determining sediment transport rates and the stability of coastal structures, as well as in storm surge and wave modeling. Accurate estimation of bed shear stress in engineering practice is still a challenge in unsteady flows (Guard et al., 2010; Sumer et al., 2008 and 2010), where bed shear stress is mostly estimated from the free stream velocity and friction coefficients. Reliable estimation of bed shear stress is necessary to predict sediment transport and related scour, deposition and morphology change (Wilcock, 1996). Shear stress developed within the bed also influence the stability of submarine sediment deposits, and the total shearing force on the sediment from both pressure gradients and skin friction is important (e.g., Madsen, 1974; Yamamoto, 1978). With the development of submarine mineral resources in increasing water depths, reliable estimates of the shear stress within the sediment bed are required for geotechnical analysis and the design of pipeline systems for a range of wave conditions, including tsunami and cyclones. Following the 2004 Indian Ocean tsunami, the west Australian continental shelf has been found to have higher tsunami hazard potential than previous estimates (Burbidge and Cummins, 2007). With more offshore oil and gas basins being released for exploration in deeper waters off Australian coast (Southgate, 2008), there is a necessity for ultra-long submarine pipelines extending in to water depths beyond 1000m which are prone to tsunami hazards. Solitary waves have been used as a proxy for tsunami wave forms (e.g., Goring, 1979; Synolakis and Bernard, 2006), although the accuracy of this approximation is extensively discussed by Madsen et al. (2008). In general, tsunami waves may take many shapes, but typically take the form of individual solitary waves, rather than periodic waves. Grue et al. (2008) simulated undular bores and solitary waves that were observed during the Indian Ocean tsunami event. Although near-real-time tsunami propagation modeling is being perfected (Tang et al., 2009), the effects of tsunami on the bed and submarine infrastructure are not well documented and remain more uncertain.

Bed shear stress is often estimated using a friction factor and free stream velocity close to the bed (Nielsen, 1992). Shear stress is most usually calculated using the quadratic drag law:

$$\tau = \frac{1}{2} \rho f u^2 \quad (1)$$

where, τ is bed shear stress, f is wave friction factor, ρ is fluid density and u is free stream velocity outside the boundary layer. Estimates of the friction velocity in the boundary

layer, u_* , ($u_* = \sqrt{\tau / \rho}$) can be obtained from a logarithmic profile fit to the velocity profile measured using different techniques and instrumentation. These methods include Laser Doppler Anemometers (LDA) (Compton and Eaton, 1996; Lim and Lewkowicz, 1986), Particle Image Velocimetry (PIV) (e.g., Jensen et al., 1989; Liu et al., 2007), Laser Doppler Velocimeter (LDV) (e.g., Skjelbreia, 1987). These methods are nonintrusive but depend on theoretical formulations to obtain bed shear stress, and have been adopted in practice due to difficulties in obtaining direct bed shear stresses from the field, as well as during laboratory experiments. A number of studies have also been performed by measuring bed shear stresses directly, either by measuring the force applied on a shear plate flush to the flume bed (Babanin et al., 2005; Ippen et al., 1955; Ippen and Mitchell, 1957; Mirfenderesk and Young, 2003; You and Yin, 2007) or by measurements of displacement of a shear plate on the bed (Barnes and Baldock, 2007; Barnes et al., 2009; Grass et al., 1995; Guard et al., 2009; Riedel and Kamphuis, 1973). Hot-film probes have been used to measure the shear stresses in water tunnels (e.g., Sumer et al., 1993) wherein the shear stress is measured as a function of heat exchange in the boundary layer. However, in hot-film method, the static calibration may not be same as a dynamic one since the temperature field may change during calibration (Carstensen et al., 2010).

A majority of the laboratory studies are dedicated to measurements of bed shear stress under periodic waves. Direct measurements of bed shear stress under solitary waves or bores are less common (Barnes et al., 2009; Guard et al., 2009; Ippen et al., 1955; Ippen and Mitchell, 1957; Liu et al., 2007; Sumer et al., 2008 and 2010), and model-data comparisons are limited. Ippen et al. (1955) measured solitary wave induced bed shear stress using shear plate and a force balance. Liu et al. (2007) derived analytical solutions for boundary layer flows and bed shear stress under solitary waves while Sumer et al. (2008 and 2010) carried out U-tube experiments on laminar and turbulent solitary wave type boundary layer flows using hot-film anemometry. Barnes et al. (2009) used a shear cell to measure bed stress and friction factors for solitary bores in dam break experiments and swash flows. Guard et al. (2010) employed FFT techniques and convolution integrals to estimate bed shear stresses from time series measurements of water levels for unsteady flows.

In this study, direct measurement of the shear stress derived from shear plate displacement over a smooth bed were made, along with simultaneous measurements of water surface elevation, free stream velocity and near bed pressure under solitary waves. Compared to the studies carried out in U-Tubes (e.g., Jensen et al., 1989; Kamphuis, 1975; Sumer et al., 1993),

where the flow is uniform in the flow direction, the present study is carried out in a wave flume where the flow is non-uniform along the flow direction, as for natural waves. In the real world applications of sediment transport or submarine structural or foundation design, the total stresses on the sea bed sediments are appropriate instead of considering only the bed shear stress generated by the boundary layer flows. This is because inertial forces impose additional loads on individual grains, as well as layers of sediment (Hsu and Hanes, 2004; Nielsen, 1992; Sleath, 1999; Teakle and Nielsen, 2003). Therefore, measurements of total force acting on the bed due to waves and the associated friction factors are of importance and are also considered in this paper. Developing and verifying the shear cell technique for transient waves over smooth beds is also necessary prior to application of the method to rough beds. Shear stresses in rough bed conditions are yet to be measured by hot-film techniques. Further, most previous estimates of the skin shear friction factors normalize the estimated shear using the maximum wave velocity in the quadratic drag law Eq.(1), which ignores any phase difference between the maximum velocity and maximum bed shear stress. For periodic waves, this is appropriate, but the resulting friction factors are strictly only valid for waves with the same phase lag between velocity and bed shear stress. For solitary waves this phase difference also occurs (e.g., Ippen et al., 1955; Liu et al., 2007; You and Yin, 2007). Therefore, the differences between friction factors obtained using both the maximum velocity and local (instantaneous velocity) are also presented. Analytical modeling of bed shear stress using the methods outlined in Liu et al. (2007) and Guard et al. (2010) is carried out to compare the model results with measurements. This paper is organized as follows: section 2 presents the methodology and data analysis techniques. The modeling approach is presented in section 3. Section 4 presents the experimental results and model-data comparisons, with final conclusions in section 5.

2. METHODOLOGY

2.1 Experimental setup and instrumentation

Barnes and Baldock (2009) developed a shear cell of similar design to that of Grass et al. (1995). The same shear cell was used for the present experiments. The shear cell consists of a 100mm long, 250mm wide and 1.21mm thick smooth plate supported on thin tubular sway legs, with displacement measured by an eddy-current sensor which resolves plate movement to 0.001 mm. Barnes and Baldock (2009) made extensive measurements of total shear and

bed shear under dam-break waves, breaking bores and swash zone flows. The present experiments were carried out in the tsunami wave flume in the UQ Gordon McKay hydraulics laboratory. The wave flume was equipped with a computer-controlled piston wave-maker having a maximum stroke length of 1.2m and capable of generating most types of waves including solitary waves and bores. The experimental setup consisted of a horizontal flat bed from the wave-maker for a distance of 9.8m (or 11m when the wave-maker retracts to its farthest position), followed by a 1:10 sloping bed up to a distance of 1.6m, and further section of horizontal flat bed for 7m. This experimental model was set up to represent a continental slope and shelf region (Fig. 1). Data from the horizontal section of the flume before the slope is presented here. The water depths for different experiments ranged from 0.105m – 0.21m. All tests were carried out with smooth flume bed made of fixed, impermeable marine plywood. The shear plate apparatus was fixed firmly and flush with the flume bed so that the shear plate displaces when an external force is applied. Microsonic[®] ultrasonic wave gauges were used to measure the wave heights. DRUCK[®] pressure transducers were used to measure the pressure within the shear cell and SONTEK[®] 2D Acoustic Doppler Velocimeter was used to measure the flow velocities. All instruments synchronously measured at 50Hz with the wave generation program, and the data was acquired using a National Instrumentation[®] data acquisition system. Wave heights were measured above the shear plate apparatus with two wave gauges placed 10cm apart which coincide with the edges of the shear plate on the flume bed. Two pressure transducers were placed within the cell on either side of the shear plate apparatus, about 2.4cm below the shear plate to measure the pressure within the cell.

2.2 Wave conditions

The methods outlined in Goring and Raichlen (1980) and Baldock et al. (2009) were used to generate the wavemaker displacement functions. Different amplitudes and periods/wavelengths were generated by varying the stroke length and celerity of the wavemaker. High celerity resulted in the generation of solitary bores (broken waves), whereas lower celerities gave smooth solitary waves. Only non-breaking waves are considered here. The wavemaker displacement functions and examples of the typical solitary waves generated are shown in 0. A total of 84 waves were generated that are considered in this study, a summary of the conditions is given in Table 1, which is also referred back to in later sections.

2.3 Analysis techniques

2.3.1. Reynolds number

For monochromatic waves, an appropriate Reynolds number can be based on wave amplitude and a velocity obtained from the wave frequency (e.g., Nielsen, 1992). However, the wave frequency is not well defined for solitary waves. Sumer et al. (2010) used an appropriate theoretical wave fitted to the measured wave profile, thereby obtaining a wave period from the theoretical wave. This method is useful only if the measured wave perfectly fits the theoretical profile. However, not all waves fit the theoretical solitary wave profile. Here, the Reynolds number (R_e) for the solitary waves is estimated using the measured free stream velocity (u), the semi-excursion length (A) of the water particles, and kinematic viscosity (ν):

$$R_e = \frac{Au}{\nu} \quad (2)$$

In order to estimate R_e , the semi-excursion length of the water particles needs to be estimated properly for the solitary waves. This semi-excursion of the water particle for each of the waves was estimated by integrating the velocity time-history from an initial velocity (2.5 % of the maximum velocity) to the maximum velocity, as illustrated in Fig. 3. In order to check the method adopted to estimate the semi-excursion lengths, measurements of particle excursion in the wave flume were made for 20 different waves. The excursion of neutrally-buoyant spheres (~0.0125m diameter) placed on the flume bed was recorded using a video camera and the distance travelled by these particles from their initial position to final position through the wave propagation was measured.

2.3.2 Shear stress

The temporal horizontal displacement of the shear plate is measured in the experiments and converted to the total shear force (τ_T) exerted on the shear plate through the known force-displacement calibration as explained by Barnes et al (2009). The total force (τ_T) comprises of bed shear stress, τ , as well as an inertial or Froude-Krylov force acting over the thickness of the plate t_p (Eq. 3), which is generated by the pressure gradient in the free stream. (Barnes

et al., 2009; Grass et al., 1995; Ippen and Mitchell, 1957; Riedel, 1972). The pressure gradient force can be written as an effective additional pressure gradient stress, τ_{pr} , on the plate, and which is equivalent to the pressure gradient induced stress at a horizontal plane within a sediment bed. If the pressure is hydrostatic then Eq. (3) simplifies to Eq. (4), where η is the surface elevation. The skin shear stress can be obtained by deducting the pressure gradient force (τ_{pr}) from the total shear force using Eq. (5).

$$\tau_{pr} = -\frac{\partial P}{\partial x} t_p \quad (3)$$

$$\tau_{pr} = -\rho g \frac{\partial \eta}{\partial x} t_p \quad (4)$$

$$\tau = \tau_T - \tau_{pr} \quad (5)$$

The shear cell provides a direct measure of the total shear force and stresses exerted by the flow on the finite thickness of the plate. However, the bed stress estimates are subject to inaccuracies introduced in applying Eqs. 3-5, i.e., determining the net pressure gradient induced force on the plate. The dynamic pressure was estimated from the surface elevation for non-hydrostatic conditions using Eq. (6) (Nielsen, 2009). The wave number, k was estimated using an explicit approximation to linear dispersion relation, Eq. (7) (Fenton and McKee, 1990). The estimated dynamic pressures were compared with those measured within the shear cell with good agreement and the pressure gradient across the surface of the plate was then derived from the surface elevation measurements either side of the shear plate.

$$P = \rho g \left[d + \frac{\eta}{\cosh(kd)} \right] \quad (6)$$

$$k = \frac{\omega^2}{g} \left[\coth(\omega \sqrt{d/g})^{3/2} \right]^{2/3} \quad (7)$$

where, P is pressure, d is water depth, g is acceleration due to gravity, ρ is fluid density, η is surface elevation, k is wave number, ω is angular frequency. However, estimates of the dynamic pressure gradient within the cell were only about 30% of those outside the cell. Assuming a linear decay in the pressure gradient across the plate, this reduces the overall estimated pressure force on the plate to 65% of the maximum possible force. This calibration coefficient has been applied to obtain the present estimated bed shear stresses, and its effect is illustrated later in Fig. 8.

3. SHEAR STRESS MODELING

The bed shear stress was modeled using the theory and convolution models for solitary and transient waves developed by Philip F. Liu and his co-workers (Liu and Orfila, 2004; Liu et al., 2007; Liu et al., 2006; Orfila et al., 2007; Torsvik and Liu, 2007). Using a perturbation expansion for the velocity field in the bottom boundary layer, Liu and Orfila (2004) developed depth integrated continuity and momentum equations including the effects of turbulent bottom boundary layer for transient long waves. Liu (2006) adapted the above method for long wave propagation and employed an eddy viscosity model, as in Eq. (8), assumed to be a power function of vertical elevation, in the boundary layer.

$$\nu_t = \nu \left[\frac{z}{z_0} \right]^p \quad (8)$$

where, z_0 is roughness height, z is depth, ν is kinematic viscosity. It was also shown that to leading order bed shear stress, τ , can be expressed as convolution integral of the depth integrated averaged horizontal velocity, \bar{u} , Eq.(9), assuming the initial velocity to be zero.

$$\tau = -\frac{q(1-q)^{2q-1}}{\Gamma(q+1)} \int_0^t \frac{\partial \bar{u}(x,T) / \partial T}{(t-T)^q} dT \quad (9)$$

where, q and p are related by $q = (1-p)/(2-p)$ and Γ is the gamma function. Further, Liu et al. (2007) showed for solitary waves that nonlinear effects are insignificant and that linearized boundary layer solutions are adequate to describe the bed shear stress in the boundary layer. For a constant viscosity, ν , the bed shear stress under a long wave, assuming again the initial velocity to be zero, is given in (Eq.10).

$$\tau(t) = \rho \sqrt{\frac{\nu}{\pi}} \int_0^t \frac{\partial u / \partial T}{\sqrt{t-T}} dT \quad (10)$$

Thus the bed shear stress is the time integration of the local acceleration, which is weighted by the function $(t-T)^{-q}$ for $0 < t < T$. The relationship between p and q for $0 < p < 1$ yields the curve shown in Fig. 4; when $q = 1/2$, $p = 0$; i.e., constant viscosity. This method is so far untested for turbulent flows, where the magnitude of ν_t might depend on the bed roughness and on time scale of the wave motion (Nielsen and Guard, 2010). In this case, Eq. (10) might be modified as follows, and this model is also tested against the present data.

$$\tau(t) = \rho \sqrt{\frac{\nu_t}{\pi}} \int_0^t \frac{\partial u / \partial T}{(t-T)^q} dT \quad (11)$$

Torsvik and Liu (2007) showed that the value of the convolution integral, Eq.(12), can be calculated numerically without considering the entire time series of velocities. The convolution integral is calculated as a weighted sum (Eq.13) where coefficients are determined using Eqs.14 and 15.

$$A_c = \int_0^t \frac{\partial u / \partial T}{(t-T)^q} dT \quad (12)$$

$$\tilde{A}_{ci}^{(k)} = \sum_{j=0}^{N-1} C_j \delta u_i^{(k-j)} \quad (13)$$

where, $\delta u_i^{(k)} = \nabla \cdot u_\alpha (i \Delta x, k \Delta t)$, and $\tilde{A}_i^{(k)} \approx A(i \Delta x, k \Delta t)$ and the weights C_0 and C_j are determined as follows:

$$C_0 = \int_{t-\frac{1}{2}\Delta t}^t \frac{1}{(t-T)^q} dT = \frac{1}{(1-q)} \left(\frac{\Delta t}{2} \right)^q \quad \text{for } j=0 \quad (14)$$

$$C_j = \int_{t-(j+\frac{1}{2})\Delta t}^{t-(j-\frac{1}{2})\Delta t} \frac{1}{(t-T)^q} dT = \frac{1}{(1-q)} \left(((j+1/2)\Delta t)^{(1-q)} - ((j-1/2)\Delta t)^{(1-q)} \right) \quad \text{for } j>0; \quad (15)$$

It should be noted that the accuracy of the approximation of the integral may depend on the value of q , but this has not been investigated further here. In this study half the record length has been used to estimate the weights C_0 and C_j .

For the convolution approach, the pressure variation was obtained using an appropriate impulse response function (Eq. 16), and since the water surface elevation height is measured in the time domain, it was transformed into the spatial domain by assuming that the wave travels with constant speed, thereby $dt = dx / \sqrt{gd}$ (Guard et al., 2010).

$$P(t) = \rho g \left[d + \int_{-3d}^{3d} \frac{\eta(x)}{2d \cosh \frac{\pi(x-x')}{2d}} dx \right] \quad (16)$$

Three different approaches were used in estimating the bed shear stress. The first approach considered the convolution models above with laminar conditions, where $q = 1/2$, or $p = 0$, in Eq.8, which gives constant kinematic viscosity in Eq.10. This approach is further referred to as the Conv-1 model. In the second approach, referred as the Conv-2 model, the convolution approach was modified as for turbulent flows, by taking $q=1/8$ and an eddy viscosity which is a function of the bed shear stress itself (Eq.17). The shear velocity, u_* , is estimated using Eq.18. This method is analogous to steady flow conditions.

$$\nu_t = 0.45 u_* z_1 \quad (17)$$

$$u_* = \sqrt{\frac{|\tau|}{\rho}} \quad (18)$$

The third approach is taking $q = 1/8$ and the eddy viscosity as given by Liu (2006) (Eq. 19). The parameter z_1 is estimated using the roughness, r , of the shear plate, taken as 0.015mm, and utilizing the semi excursion length as in Eq.20 (c.f.,Nielsen, 1992). This approach is referred as the Conv-3 model.

$$v_i = \frac{7\nu}{8.7} \left(\frac{z_1 u_*}{\nu} \right)^{6/7} \quad (19)$$

$$z_1 = 0.09 \sqrt{r/A} \quad (20)$$

Measured velocities from the wave flume experiments were used in all the convolution models. The phase differences between the measured maximum values of velocity and (a) measured maximum positive total shear stress, $\tau_{T,\max}$ and (b) modeled maximum positive bed shear stress, τ_{\max} are also estimated for model-data comparisons. The time of occurrence of maximum velocity is taken as a reference time and the differences in the time of maxima of $\tau_{T,\max}$ and τ_{\max} , with respect to the reference time is calculated. In order to convert time difference in seconds to degrees, the wave period is estimated by considering the time elapsed between 2.5% of the maximum velocity and time of occurrence of maximum velocity in the forward direction and this time corresponds to 180° . Thereafter, the phase lag between u_{\max} and either $\tau_{T,\max}$ or τ_{\max} are converted to degrees of a notional wave period for comparison with observations from other experiments and wave types.

4. RESULTS AND DISCUSSION

The data presented here are for a flat smooth bed and non breaking solitary type waves. The measured and derived parameters of maximum wave height to water depth ratio (γ), Reynolds numbers (Re), maximum free stream velocity (u_{\max}), semi-excursion length to depth ratio (A/d), maximum positive total shear stress ($\tau_{T,\max}$) and maximum negative total shear stress ($\tau_{T,\min}$, hereinafter referred as minimum total shear stress) are presented in Table 1. In order to check the theoretical estimates of Re , the predicted excursion lengths were compared with measured excursion lengths obtained from the video measurements of particle movements described in section 2.3.1. The estimated excursion lengths match very well with

the measured excursion lengths (Fig. 5). Thus, the method adopted to estimate the excursion length and R_c is considered acceptable and reliable. The relationship between Froude number, F_r , and γ indicates a linear relationship following linear wave theory ($\frac{u}{\sqrt{gd}} = \frac{H}{d}; F_r = \gamma$) (Jonsson et al., 2000), up to a value of 0.225 for both F_r and γ (Fig. 6). Thereafter, a distinct breakpoint was observed (i.e., at both F_r and $\gamma = 0.225$) indicating a possible change in flow regime. The best fit for the higher values of F_r indicate $F_r = 0.6\gamma + 0.08$. Even though a change in flow regime is seen at F_r and $\gamma > 0.225$, the maximum total shear stress measured ($\tau_{T,max}$) from the shear plate is observed to be linearly proportional to γ , where $\tau_{T,max} = 3.5\gamma$ (Fig. 7).

A typical time-history of a typical solitary wave surface elevation, corresponding free stream velocity and the total shear stress are show in Fig. 8. As has been observed by earlier researchers (e.g., Ippen et al., 1955; Liu et al., 2007), the total shear stress leading the free stream velocity is clearly observed (Fig. 8(a)). However, the free stream velocity is always positive during the entire propagation of the solitary wave over the shear plate, but the total stress reverses sign. This can be attributed to the adverse pressure gradient after the wave crest passes, and the pressure gradient force becomes negative (upwave) during the deceleration phase of the wave motion (Sumer et al., 2008 and 2010). Deduction of the pressure gradient force, τ_{pr} , from the measured total shear stress, τ_T , provides the estimated bed shear stress or skin shear stress, τ , which is shown in Fig. 8(b). The prominent negative values observed in τ_T is still present but less pronounced in τ , which supports the argument that the effect of pressure gradient force during deceleration phase influences the total shear stress to a much larger extent than the skin shear term. Also, the phase difference between the maximum value of free stream velocity, u_{max} , (which is in phase with the water surface elevation) and τ_T is greater than the phase difference between u_{max} and τ . Fig. 8 also includes a set of numbered points (1 to 6) during the wave phase which illustrate the different maxima and minima of τ_T and τ , and the values of τ_T and τ at the time of maximum velocity. These definitions are used in later discussion. Fig. 8(c) illustrates the different estimates of τ for this case when assuming different calibration coefficients for the pressure gradient component. The value of τ_{max} is insensitive to the calibration term, but the phase difference and minimum stress are significantly changed. The good agreement between the skin shear stress estimates based on applying 65% of the pressure gradient force and the Liu

et al. (2007) laminar solution suggests this correction is appropriate. Comparison of the maximum and minimum values of measured τ_T (Fig. 9) show that they are linearly proportional for all the tests carried out in this study and the maximum values of τ_T were about 1.46 times greater than the corresponding minimum values of τ_T .

In order to compare the measurements and the model results for total shear stress, the maximum values of the measured and model shear stresses are further considered. Predicted skin shear stress, τ , for the three models discussed earlier (viz., Conv-1, Conv-2 and Conv-3) was combined with predicted pressure gradient force, τ_{pr} , to obtain predicted total shear stress from each model. These calculations are relevant for estimates of the total shear stress on a layer of marine sediment or a sheet flow layer of given thickness. Maximum values of predicted τ_T are compared with the maximum values of measured τ_T in Fig. 10, which shows that the predicted τ_T from Conv-1, in general, predicts the data well compared to the other two models. However, all the three models are seen to scatter at higher values of τ_T . Estimates of τ_T from Conv-1 are found to provide the best correlation with τ_T from the measurements. Predicted skin shear stress, τ , from Conv-1 was compared with τ derived from the measurements, with generally good agreement, although this model underestimates τ by about 4% (Fig. 11) which could be due to regime change from laminar to transitional or transitional to turbulent.

Since the forces acting on the bed comprises of both pressure gradient force and bed shear stresses, it might be appropriate to consider the total force to estimate the friction factors, particularly in cases where the wave induced pressures are significant. However, in most of the literature the friction factor (f) is estimated using skin shear stress alone, ignoring the pressure gradient force. In this study friction factors are estimated using Eq. 21, where both skin shear stress and total shear stress are used for τ_m . For the cases where τ_T is used, the factors are termed as “total force coefficients” (f_T) whereas they are termed the usual “friction factors” where τ is used.

$$f_T, f = \frac{2\tau_m}{\rho U^2} \quad (21)$$

In order to understand the differences in estimating f_T or f from Eq. 21, six prominent points, as defined in Fig. 8, are considered. Point-1 corresponds to the maximum value of the measured total shear stress, point-2 corresponds to the total shear stress at the time of maximum velocity and point-3 corresponds to the minimum value of measured total shear

stress (Fig. 8(a)). Point-4 corresponds to the maximum value of estimated skin shear stress, point-5 corresponds to the skin shear stress at the time of maximum velocity and point-6 corresponds to the skin shear stress at the time of maximum total shear stress (Fig. 8(b)). Measured total shear stress, τ_T or skin shear stress, τ , are appropriately used to estimate corresponding “total force coefficients” or “friction factors”. Also the velocity that is used in Eq. 21 is either the maximum velocity or the instantaneous velocity. This analysis differs from that of Sumer et al. (2010) and conventional analysis of periodic waves. In those instances, U in Eq. 21 is taken to be the maximum velocity, even though this does not necessarily correspond to the velocity at the time of the measured maximum shear stress. The total stress coefficients are plotted as function of Reynolds number in Fig. 12-14. It should be noted that the total force includes skin shear stress and hence the wave friction factor is included in the total force coefficients. Total force coefficients at maximum total shear stress are compared with the total force coefficients obtained at minimum total shear stress and presented in Fig. 15. Friction factors as function of Reynolds number with the Stanton-type wave friction diagram of Kamphuis (1975) in the background are presented in Fig. 16-18.

The total force coefficients at maximum τ_T (point-1) using both maximum velocity and corresponding instantaneous velocity are presented in Fig. 12. The total force coefficients estimated using their corresponding instantaneous velocity ($f_{T1,u}$) were observed to be on the lower limit of the rough turbulent regime, which can be described by a function $f_{T1,u} = 8/\sqrt{R_e}$. In contrast, the same coefficients (at point-1) estimated using maximum velocity ($f_{T1,umax}$) are found to be about half the value of $f_{T1,u}$ and these coefficients can be described by a function $f_{T1,umax} = 3.5/\sqrt{R_e}$. The total force coefficients estimated at time of maximum velocity (point-2) were found to be scattered below the theoretical line for smooth laminar flow (Nielsen, 1992) and are not following any particular trend (Fig. 13). This could be expected based on the typical phase relationships shown in Fig. 8, i.e. for transient waves there is no particular relationship between the maximum total stress and the maximum velocity. The minimum total force coefficients at point-3, estimated using the corresponding instantaneous velocity ($f_{T3,u}$) were observed to be similar to but slightly less than those for the maximum total stress $f_{T1,u}$ (Fig. 14). These coefficients can be described by a function $f_{T3,u} = 6/\sqrt{R_e}$. Similarly the coefficients at point-3 estimated using maximum velocities ($f_{T3,umax}$) can be described by $f_{T3,umax} = 2.5/\sqrt{R_e}$. The total force coefficients estimated using the maximum velocity were compared and coefficients for the maximum

stress were about 1.34 times those for the minimum stress (Fig. 15), as expected from the data in Fig. 9.

Following a similar method and nomenclature, friction factors are derived at points 4, 5 and 6 on the waveform (c.f Fig.8). The friction factors derived from maximum shear stress (point 4) and maximum velocities were 40% less than the factors derived from corresponding velocities (Fig. 16). The friction factors at point-4 using maximum velocity can be described by $f = 2.5/\sqrt{R_e}$ whereas using instantaneous velocities the friction factor can be described by $f = 3.5/\sqrt{R_e}$. Friction factors at point-5 were observed to be on the smooth laminar to transition region on the Kamphius plot (Fig. 17) and these can be described by the function $f = 2/\sqrt{R_e}$. The friction factors at the time of maximum total stress, point 6 (Fig. 18), estimated using corresponding velocities, showed similar trends to those at points 4 whereas using maximum velocities showed closer trend with those at point-5.

In general, the friction factors estimated in this study are found to be within the laminar to transition flow regime, with an upper bound described by $f = 3.5/\sqrt{R_e}$ and a lower bound of about $1.75/\sqrt{R_e}$, similar to the conventional values for smooth laminar flow. However, the lower bound is not significant as noted above. The results suggest that the friction factors could be estimated by simplified functions of R_e , rather than the full convolution model, provided the appropriate velocity is adopted. However, such an approach may not be valid of transient waves of arbitrary form and the full model approach is preferred.

A further test of the models is provided by considering the measured and predicted phase difference between the stress and free stream velocity. The measured phase differences obtained between u_{max} and $\tau_{T,max}$ show that these lie between $\sim 40^\circ$ and $\sim 70^\circ$ with a median value around 50° (Fig. 19), with a positive difference indicating the total shear stress leads the velocity. In contrast, the measured phase differences between u_{max} and τ_{max} vary between 5° and about 50° , with a median value of 30.8° and with larger scatter. The modeled phase differences for the maximum skin friction stress are shown in Fig. 20, and the model and data are in good agreement, with a predicted median phase of 29.65° which is similar to that of measurements as well as similar to that observed by Sumer et al. (2008 and 2010). This phase lead is a little smaller than that observed for sinusoidal waves for both laminar and turbulent flow conditions. A possible explanation is that the water particle semi-excursion lengths are proportionately greater under solitary waves of a given height than for sinusoidal waves of

the same height. Hence, the boundary layer has more distance to develop toward quasi-steady conditions (no phase differences) before maximum velocity and stress occur.

5. CONCLUSIONS

Direct measurements of total shear stresses due to non-breaking solitary type wave propagation on a flat smooth bed were carried in a wave flume. The results on the Froude number and relative water depth showed that the flow regime changes beyond a Froude number of 0.225 in other words the water particle velocities do not obey linear wave theory beyond Froude number of 0.225. However, the measured maximum total shear stresses were still observed to be linearly proportional to relative water depth.

Semi excursion lengths were estimated by integrating the velocity profile up to 2.5% of the maximum velocity which provided reliable comparison with measured excursion lengths, thereby better estimates of Reynolds numbers. The Reynolds numbers obtained from the tests carried out in this study ranged between 8900 and 67200.

Both the total shear stress and skin shear stress change sign during the deceleration phase of the wave, and to a greater extent for the total stress, which is attributed to the pressure gradient force from the curvature of the surface elevation. Convolution integration on the acceleration in time domain was used to estimate the bed shear stress with different eddy viscosity models. Theoretical estimates of bed shear stress were well correlated with the measurements and generally lower than the measured data by 4%, but this is within the calibration accuracy of the shear cell and velocity measurements.

Total force coefficients derived from the total shear stress measurements and different velocities showed that coefficients estimated using corresponding velocities resulted in higher values compared to those derived from maximum velocities. This is because of the phase differences between stress and velocity. The total force coefficients obtained for maximum positive total shear stress were about 1.34 times those for the minimum negative total shear stress.

Friction factors estimated at maximum velocity showed similar trend to the theoretical oscillatory flow results of Kamphuis (1975). However, friction factors derived at other points showed higher estimates compared to those at maximum velocity indicating that appropriate friction factors needs to be employed to obtain reliable estimates of shear stress. The results showed that these friction factors can be described by simple functions of Reynolds numbers.

The median phase difference between total shear stress and maximum velocity was about 50° where the phase difference between maximum shear stress and maximum velocity was about 30° .

6. ACKNOWLEDGEMENTS

Jaya Kumar Seelam is an Endeavour International Postgraduate Research Scholar at the UQ. The work carried out in this paper is part of a research project supported by CSIRO-Australia's Flagship Cluster Grant under Wealth from Oceans - Pipeline Hazards program. Graham Illidge, Clive Booth and Ahmed Ibrahim are acknowledged for their technical help during wave flume experiments at the UQ. Authors acknowledge the anonymous reviewers in improving the manuscript. NIO contribution number (to be filled up after receiving manuscript acceptance intimation).

7. REFERENCES

- Babanin, A.V., Young, I.R. and Mirfenderesk, H., 2005. Field and laboratory measurements of wave-bottom interaction, 17th Australasian Coastal and Ocean Engineering Conference, Adelaide, pp. 293-298.
- Baldock, T.E., Cox, D., Maddux, T., Killian, J. and Fayler, L., 2009. Kinematics of breaking tsunami wavefronts: A data set from large scale laboratory experiments. *Coastal Engineering*, 56(5-6): 506-516.
- Barnes, M.P. and Baldock, T.E., 2007. Direct Bed Shear Stress Measurements in Laboratory Swash. *Journal of Coastal Research*, SI 50: 641-645.
- Barnes, M.P., O'Donoghue, T., Alsina, J.M. and Baldock, T.E., 2009. Direct bed shear stress measurements in bore-driven swash. *Coastal Engineering*, 56: 853-867.
- Burbidge, D. and Cummins, P., 2007. Assessing the threat to Western Australia from tsunami generated by earthquakes along the Sunda Arc. *Natural Hazards*, 43(3): 319-331.
- Carstensen, S., Sumer, B.M. and Fredsøe, J., 2010. Coherent structures in wave boundary layers. Part I. Oscillatory motion. *Journal of Fluid Mechanics*, 646: 169-206.
- Compton, D.A. and Eaton, J.K., 1996. A high-resolution laser Doppler anemometer for three-dimensional turbulent boundary layers. *Experiments in Fluids*, 22(2): 111-117.
- Fenton, J.D. and McKee, W.D., 1990. On calculating the lengths of water waves. *Coastal Engineering*, 14: 499 - 513.
- Goring, D.G., 1979. *Tsunamis - The propagation of long waves on to a shelf*, California Institute of Technology, Pasadena, 337 pp.
- Goring, D.G. and Raichlen, F., 1980. The generation of long waves in the laboratory., 7th Coastal Engineering Conference. ASCE, pp. 763-784.
- Grass, A.J., Simons, R.R., Maciver, R.D., Mansour-Tehrani, M. and Kalopedis, A., 1995. Shear cell for direct measurement of fluctuating bed shear stress vector in combined wave/current flow. In: P.o.X.I. Congress (Editor), *Hydraulic Research and its Applications next Century - HYDRA 2000*, pp. 415-420.

- Grue, J., Pelinovsky, E.N., Fructus, D., Talipova, T. and Kharif, C., 2008. Formation of undular bores and solitary waves in the Strait of Malacca caused by the 26 December 2004 Indian Ocean tsunami. *J. Geophys. Res.*, 113.
- Guard, P.A., Baldock, T.E. and Nielsen, P., 2009. *Bed Shear Stress in Unsteady Flow, Coasts and Ports 2009*, Wellington, New Zealand.
- Guard, P.A., Nielsen, P. and Baldock, T.E., 2010. Bed shear stress in unsteady flow, 32nd International Conference on Coastal Engineering, Shanghai, China, pp. 1-8.
- Hsu, T.J. and Hanes, D.M., 2004. Effects of wave shape on sheet flow sediment transport. *Journal of Geophysical Research*, 109(C05025): 10.1029/2003JC002075.
- Ippen, A.T., Kulin, G. and Raza, M.A., 1955. Damping characteristics of the solitary wave. 16, Massachusetts Institute of Technology, Hydrodynamics Laboratory.
- Ippen, A.T. and Mitchell, M.M., 1957. The damping of the solitary wave from boundary shear measurements. 23, Massachusetts Institute of Technology, Hydrodynamics Laboratory.
- Jensen, B.L., Sumer, B.M. and Fredsoe, J., 1989. Turbulent oscillatory boundary layers at high Reynolds numbers. *Journal of Fluid Mechanics*, 206: 265–297.
- Jonsson, I.G., Thorup, P. and Tamasauskas, H.T., 2000. Accuracy of asymptotic series for the kinematics of high solitary waves. *Ocean Engineering*, 27(5): 511-529.
- Kamphuis, J.W., 1975. Friction factor under oscillatory waves. *ASCE Journal of waterway, port, coastal and ocean engineering*, 101(WW2): 135-144.
- Lim, F.K. and Lewkowicz, A.K., 1986. Investigation by laser Doppler anemometry of the turbulent flow around cylindrical obstacles on a rough surface. *International Journal of Heat and Fluid Flow*, 7(2): 102-108.
- Liu, P.L.F., 2006. Turbulent Boundary-Layer Effects on Transient Wave Propagation in Shallow Water. *Proceedings of the Royal Society London A*, 462(2075): 3481-3491.
- Liu, P.L.F. and Orfila, A., 2004. Viscous effects on transient long-wave propagation. *Journal of Fluid Mechanics*, 520(-1): 83-92.
- Liu, P.L.F., Park, Y.S. and Cowen, E.A., 2007. Boundary layer flow and bed shear stress under a solitary wave. *Journal of Fluid Mechanics*, 574: 449-463.
- Liu, P.L.F., Simarro, G., Vandever, J. and Orfila, A., 2006. Experimental and numerical investigation of viscous effects on solitary wave propagation in a wave tank. *Coastal Engineering*, 53(2-3): 181-190.
- Madsen, O.S., 1974. Stability of a sand bed under breaking waves, 14th International Conference Coastal Engineering. ASCE, Copenhagen, pp. 776–794.
- Madsen, P.A., Fuhrman, D.R. and Schaeffer, H.A., 2008. On the solitary wave paradigm for tsunamis. *Journal of Geophysical Research*, 113(C12): 10.1029/2008jc004932.
- Mirfenderesk, H. and Young, I.R., 2003. Direct measurements of the bottom friction factor beneath surface gravity waves. *International Journal of Applied Ocean Research*, 25: 269-287.
- Nielsen, P., 1992. *Coastal bottom boundary layers*. World Scientific, Singapore, 324 pp.
- Nielsen, P., 2009. *Coastal and Estuarine Processes*. Advanced Series on Ocean Engineering. World Scientific, New York, NJ (USA), 343 pp.
- Nielsen, P. and Guard, P.A., 2010. Vertical scales and shear stresses in wave boundary layers over movable beds, 32nd International Conference on Coastal Engineering, Shanghai, China, pp. 1-8.
- Orfila, A., Simarro, G. and Liu, P.L.F., 2007. Bottom friction and its effects on periodic long wave propagation. *Coastal Engineering*, 54(11): 856-864.
- Riedel, H.P., 1972. Direct measurement of bed shear stress under waves. Ph.D Thesis Thesis, Queens University, Kingston.

- Riedel, H.P. and Kamphuis, J.W., 1973. A shear plate for use in oscillatory flow. *Journal of Hydraulic Research*, 11: 137-156.
- Skjelbreia, J.E., 1987. Observations of Breaking Waves on Sloping Bottoms by Use of Laser Doppler Velocimetry. KH-R-48, W.M. Keck Laboratory of Hydraulics and Water Resources, California Institute of Technology, Pasadena, California.
- Sleath, J.F.A., 1999. Conditions for plug formation in oscillatory flow. *Continental Shelf Research*, 19: 1643-1664.
- Southgate, P., 2008. Offshore energy program underway. In: *GeoScience-Australia* (Editor), AUSGEO NEWS, pp. 3.
- Sumer, B.M., Arnskov, M.M., Christiansen, N. and Jorgensen, F.E., 1993. Two-component hot-film probe for measurements of wall shear stress. *Experiments in Fluids*, 15: 380-384.
- Sumer, B.M., Jensen, P.M., Soerensen, L.B., Fredsøe, J., Liu, P. L. F. and Carstensen, S., 2010. Coherent structures in wave boundary layers. Part 2. Solitary motion. *Journal of Fluid Mechanics*, 646: 207-231.
- Sumer, B.M., Jensen, P.M., Sorensen, L.B., Fredsøe, J. and Liu, P.L.F., 2008. Turbulent Solitary Wave Boundary Layer. In: T.I.S.o.O.a.P.E. (ISOPE) (Editor), Eighteenth (2008) International Offshore and Polar Engineering Conference, Vancouver, BC, Canada, pp. 775-781.
- Synolakis, C.E. and Bernard, E.N., 2006. Tsunami science before and beyond Boxing Day 2004. *Philosophical Transactions - A Math Physics Engineering Science*, 364(1845): 2231-2265.
- Tang, L., Titov, V.V. and Chamberlin, C.D., 2009. Development, testing, and applications of site-specific tsunami inundation models for real-time forecasting. *Journal of Geophysical Research*, 114(C12025): 1-22.
- Teakle, I. and Nielsen, P., 2003. Two-phase modelling of vertical sediment fluxes in oscillatory sheet flow, Coastal sediments '03, Florida, USA, pp. 14.
- Torsvik, T. and Liu, P.L.F., 2007. An efficient method for the numerical calculation of viscous effects on transient long waves. *Coastal Engineering*, 54(3): 263-269.
- Wilcock, P.R., 1996. Estimating Local Bed Shear Stress from Velocity Observations. *Water Resour. Res.*, 32(11): 3361-3366.
- Yamamoto, T., 1978. Sea bed instability from waves, 10th Offshore Technology Conference, Houston, pp. 1819-1824.
- You, Z.-J. and Yin, B.S., 2007. Direct Measurement of Bottom Shear Stress under Water Waves. *Journal of Coastal Research*, SI 50: 1132 - 1136.

Table 1. Range of experimental data

S.no	H/d	U	Re	$\tau_{T,max}$	$\tau_{T,min}$	A/d	S.no	H/d	U	Re	$\tau_{T,max}$	$\tau_{T,min}$	A/d
1	0.193	0.18	8923.31	0.587	0.471	0.483	43	0.195	0.22	16528.18	0.632	0.484	0.491
2	0.201	0.18	9029.55	0.816	3.832	0.479	44	0.197	0.22	16940.00	0.643	0.477	0.503
3	0.266	0.23	13830.97	0.862	0.687	0.572	45	0.308	0.32	30129.44	1.079	0.731	0.613
4	0.272	0.24	14789.60	0.871	0.699	0.590	46	0.308	0.32	29939.23	1.079	0.731	0.611
5	0.400	0.32	22971.31	1.303	1.006	0.691	47	0.160	0.19	13089.37	0.479	0.386	0.454
6	0.376	0.31	22272.88	1.278	0.973	0.677	48	0.171	0.20	13797.56	0.528	0.410	0.454
7	0.537	0.39	30578.09	1.785	1.304	0.754	49	0.316	0.32	28632.65	1.030	0.699	0.575
8	0.541	0.39	29532.74	1.764	1.298	0.731	50	0.313	0.32	29835.77	1.032	0.687	0.603
9	0.535	0.38	27794.05	1.758	1.417	0.696	51	0.541	0.50	55269.88	1.908	1.214	0.718
10	0.520	0.38	29259.15	1.753	1.390	0.736	52	0.566	0.51	57948.65	1.958	1.195	0.732
11	0.516	0.38	29200.57	1.719	1.255	0.734	53	0.387	0.39	37777.55	1.333	0.875	0.625
12	0.512	0.38	27991.28	1.690	1.225	0.702	54	0.383	0.38	39762.04	1.316	0.888	0.668
13	0.495	0.37	27908.07	1.662	1.251	0.718	55	0.192	0.22	15857.29	0.605	0.447	0.472
14	0.507	0.37	28408.34	1.662	1.260	0.735	56	0.203	0.23	16159.00	0.630	0.506	0.461
15	0.241	0.21	11971.82	0.754	0.603	0.543	57	0.126	0.17	13273.23	0.423	0.331	0.368
16	0.241	0.21	12258.98	0.744	0.602	0.558	58	0.130	0.17	11335.72	0.424	0.326	0.318
17	0.375	0.31	21278.50	1.240	0.931	0.663	59	0.161	0.21	17921.09	0.540	0.402	0.409
18	0.379	0.31	21226.10	1.239	0.941	0.662	60	0.159	0.21	18652.14	0.529	0.388	0.427
19	0.201	0.19	10128.62	0.597	0.498	0.524	61	0.242	0.29	31147.09	0.854	0.564	0.512
20	0.210	0.19	10485.64	0.672	0.519	0.516	62	0.244	0.30	33251.71	0.879	0.544	0.526
21	0.411	0.33	23049.29	1.353	1.017	0.666	63	0.340	0.39	48176.92	1.232	0.712	0.590
22	0.398	0.33	23864.45	1.331	3.772	0.696	64	0.342	0.38	45935.35	1.255	0.734	0.572
23	0.522	0.40	31133.61	1.746	3.688	0.737	65	0.441	0.44	53400.40	1.662	0.904	0.576
24	0.538	0.38	27044.64	1.745	1.267	0.681	66	0.449	0.45	59079.72	1.682	0.924	0.630
25	0.565	0.40	29231.66	1.808	1.299	0.696	67	0.291	0.35	40855.73	1.066	0.688	0.559
26	0.684	0.40	29757.50	1.772	1.248	0.709	68	0.296	0.34	40839.66	1.074	0.682	0.568
27	0.250	0.23	13854.53	0.781	0.626	0.583	69	0.356	0.40	51773.37	1.318	0.782	0.619
28	0.244	0.21	12441.04	0.762	0.603	0.551	70	0.358	0.40	50275.21	1.328	0.795	0.605
29	0.154	0.17	10736.42	0.473	0.386	0.410	71	0.160	0.20	17079.80	0.531	0.398	0.399
30	0.154	0.16	9147.79	0.463	0.370	0.371	72	0.160	0.20	16328.96	0.534	0.395	0.391
31	0.193	0.19	12461.11	0.636	0.466	0.435	73	0.247	0.29	31712.67	0.866	0.557	0.519
32	0.194	0.22	16210.06	0.634	0.482	0.478	74	0.246	0.29	31248.56	0.877	0.549	0.516
33	0.305	0.32	28486.71	1.092	0.720	0.581	75	0.120	0.16	13210.24	0.386	0.309	0.384
34	0.309	0.32	29260.26	1.076	0.736	0.592	76	0.130	0.18	13626.18	0.416	0.334	0.369
35	0.431	0.41	42100.04	1.530	0.972	0.666	77	0.231	0.30	34050.57	0.809	0.526	0.533
36	0.432	0.41	42316.26	1.554	0.981	0.674	78	0.238	0.31	33279.89	0.819	0.527	0.521
37	0.568	0.49	55228.68	2.060	1.269	0.734	79	0.424	0.48	67204.00	1.536	0.847	0.667
38	0.573	0.49	53858.74	2.059	1.266	0.713	80	0.429	0.48	67113.23	1.566	0.869	0.665
39	0.388	0.38	37005.29	1.401	0.919	0.635	81	0.290	0.36	42029.89	1.018	0.651	0.559
40	0.388	0.38	37635.86	1.399	0.922	0.637	82	0.285	0.36	42698.05	1.020	0.671	0.570
41	0.480	0.44	45680.22	1.734	1.099	0.676	83	0.158	0.21	18522.16	0.516	0.377	0.419
42	0.475	0.44	45843.28	1.737	1.068	0.674	84	0.157	0.21	20079.54	0.515	0.374	0.446

(H = wave height (m); d = water depth (m); A = semi-excursion length (m); Re = Reynolds number; U = maximum velocity (m/s); $\tau_{T,max}$ = Maximum total shear stress (Pa); $\tau_{T,min}$ = Minimum total shear stress (Pa);)

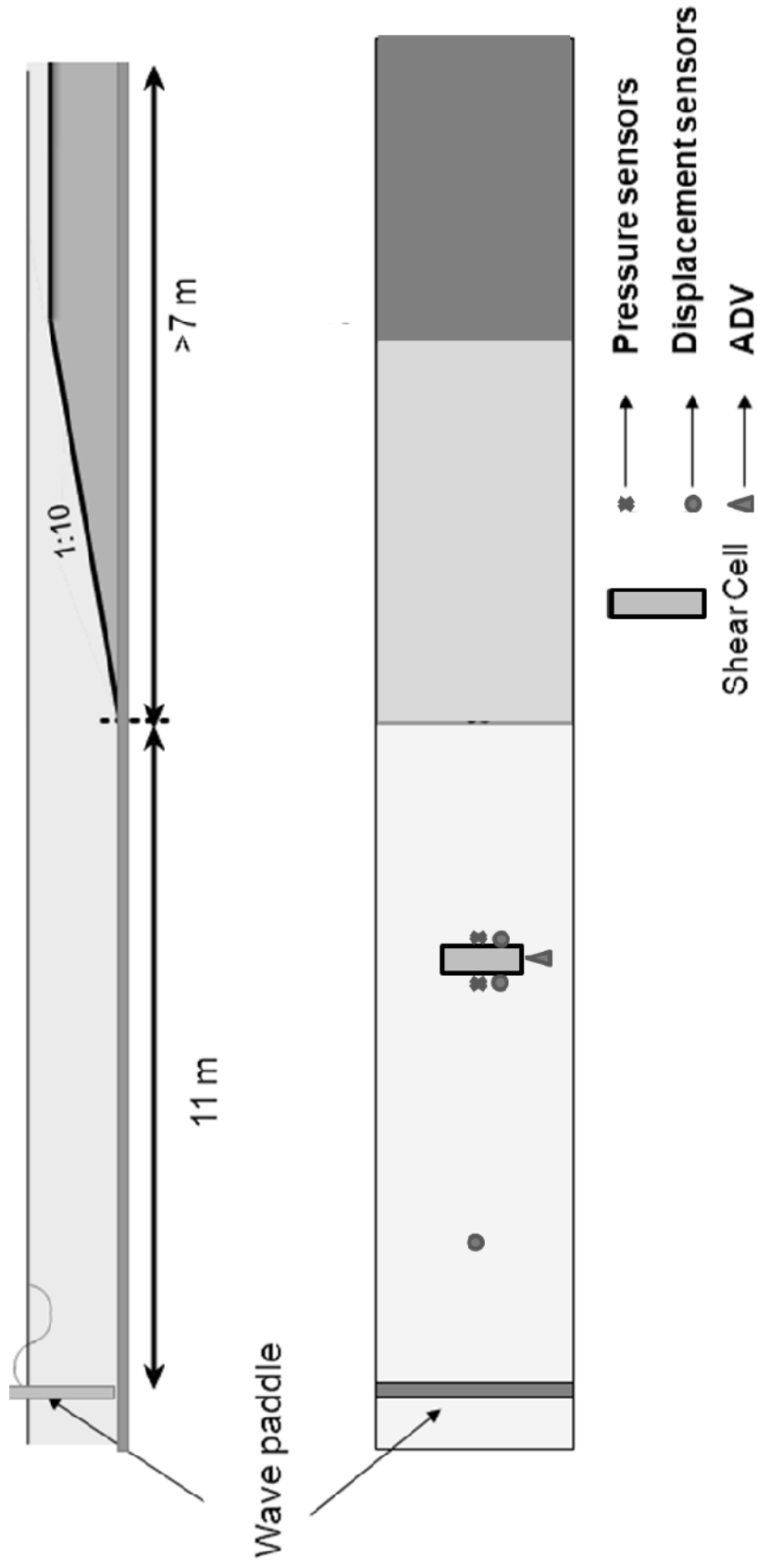
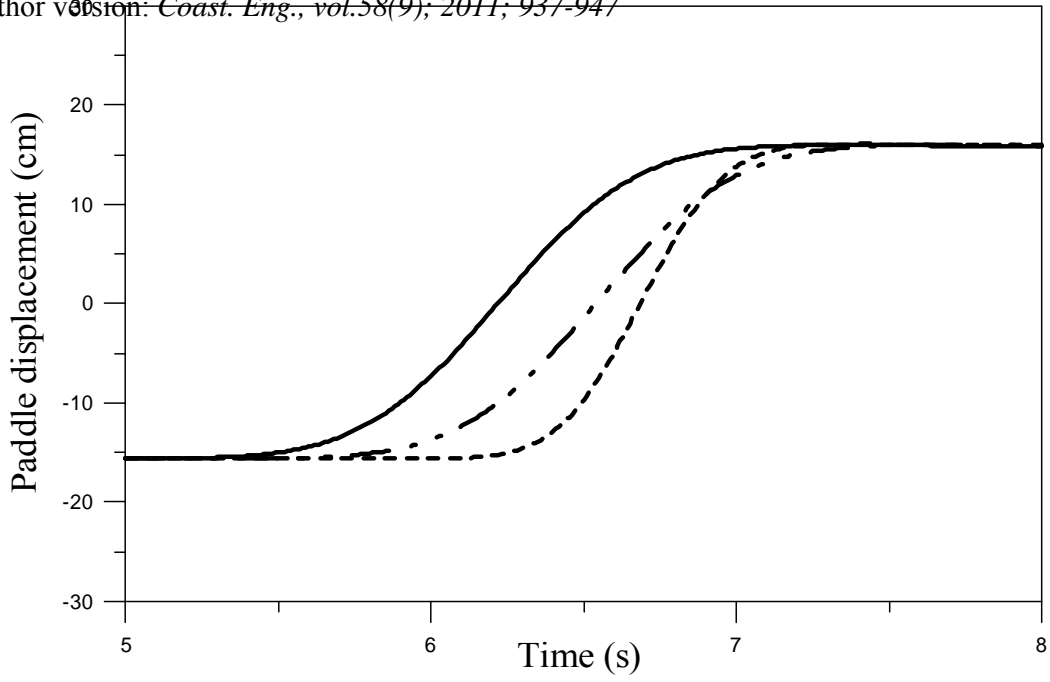
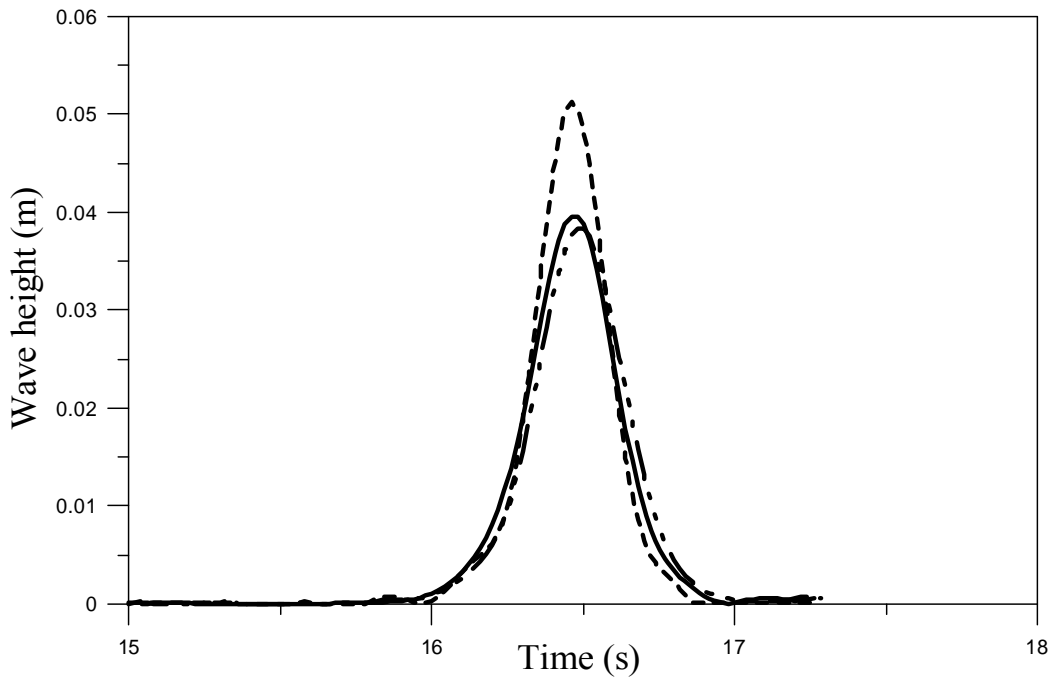


Fig. 1. Experimental setup showing locations of shear plate apparatus (shear cell), pressure sensors, ADV, wave gauges (displacement sensors) and wave paddle; (figure not to scale).



(a)



(b)

Fig. 2. Paddle displacement and corresponding wave profile generated for non-breaking solitary waves. (a) paddle displacement (b) wave profile; _____ and - - - - correspond to error wave function and _____ corresponds to solitary wave function.

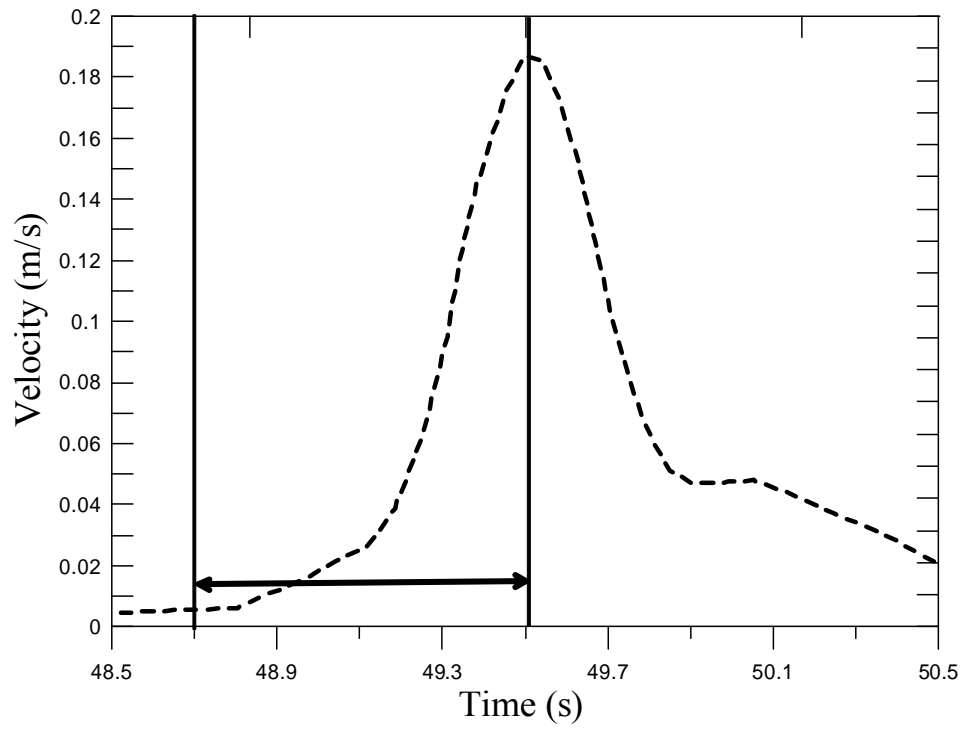


Fig. 3. Estimation of semi-excursion length (A) from time history of velocity; limits of velocity profile for semi-excursion computation are shown as vertical lines.

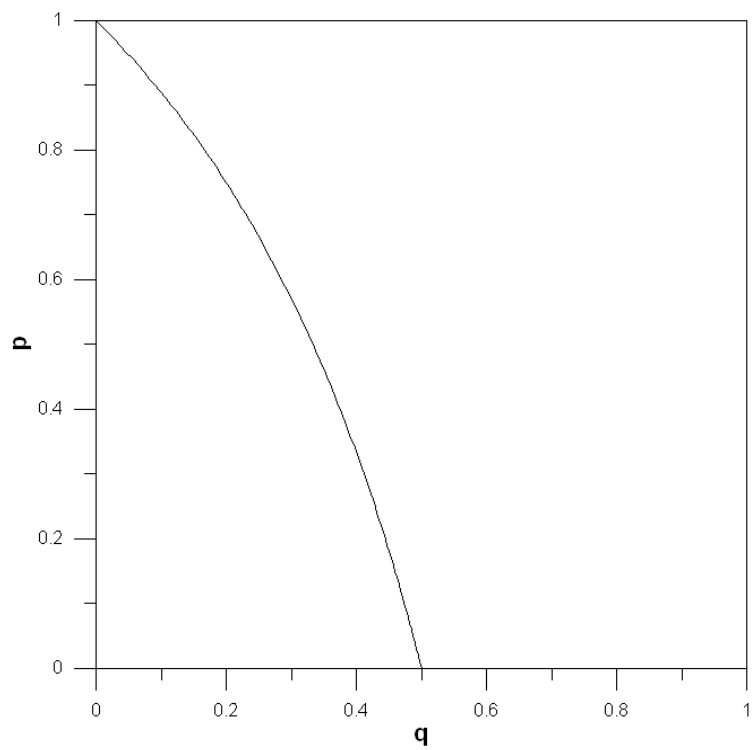


Fig. 4. Relationship between p and q.

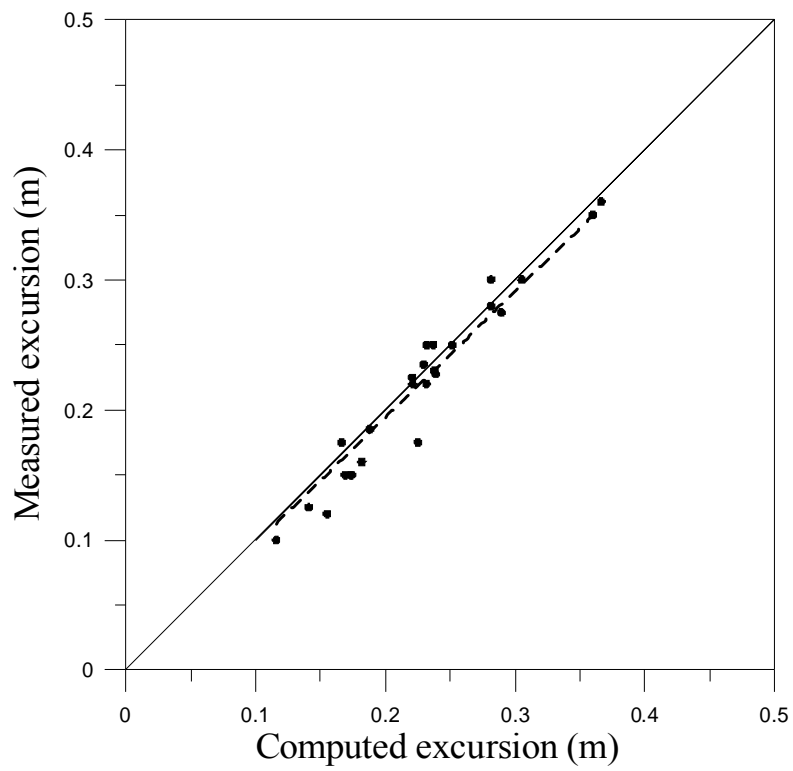


Fig. 5. Comparison of measured and estimated excursion lengths; ____ line of equality; - - - - best fit line ($R^2 = 0.995$).

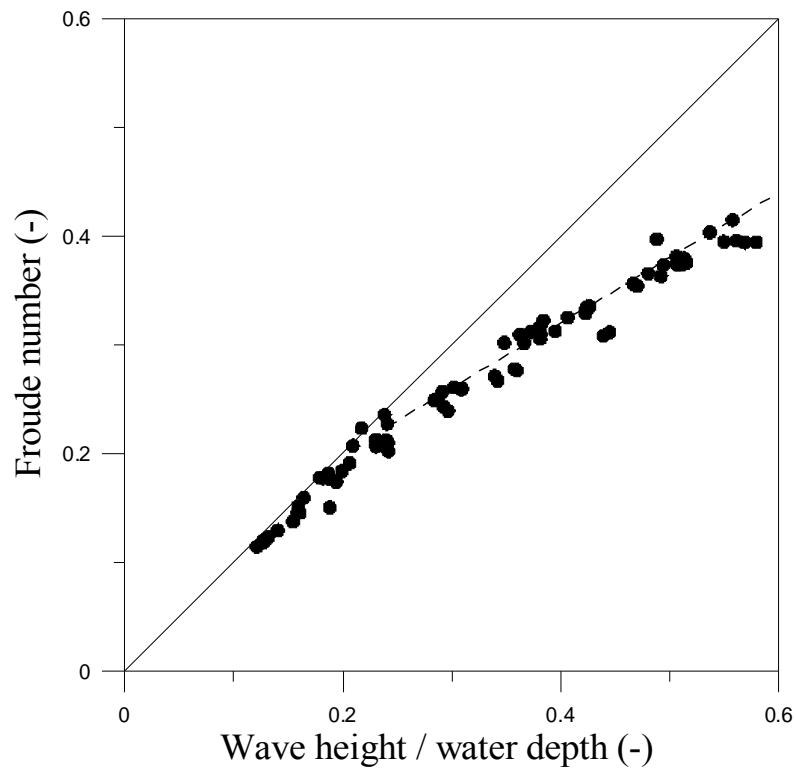


Fig. 6. Relationship between Froude number, $F_r = u_{\max} / \sqrt{gd}$ and wave height to water depth ratio, γ . Solid line is linear wave theory ($u_{\max} = \eta_{\max} \sqrt{g/d}$; $F_r = \gamma$); - - - - best fit (for $\gamma > 0.2$; $F_r = 0.08 + 0.6 \gamma$)

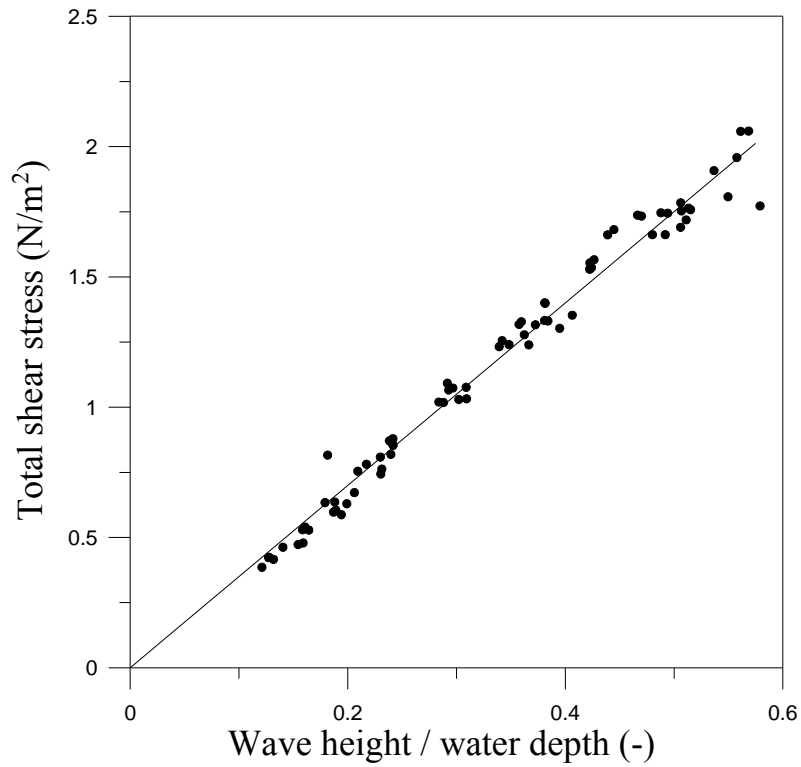


Fig. 7. Relationship between maximum measured total shear stress, τ_T and wave height to water depth ratio, γ . Solid line is line of best fit ($\tau_T = 3.5 \gamma$; $R^2 = 0.997$).

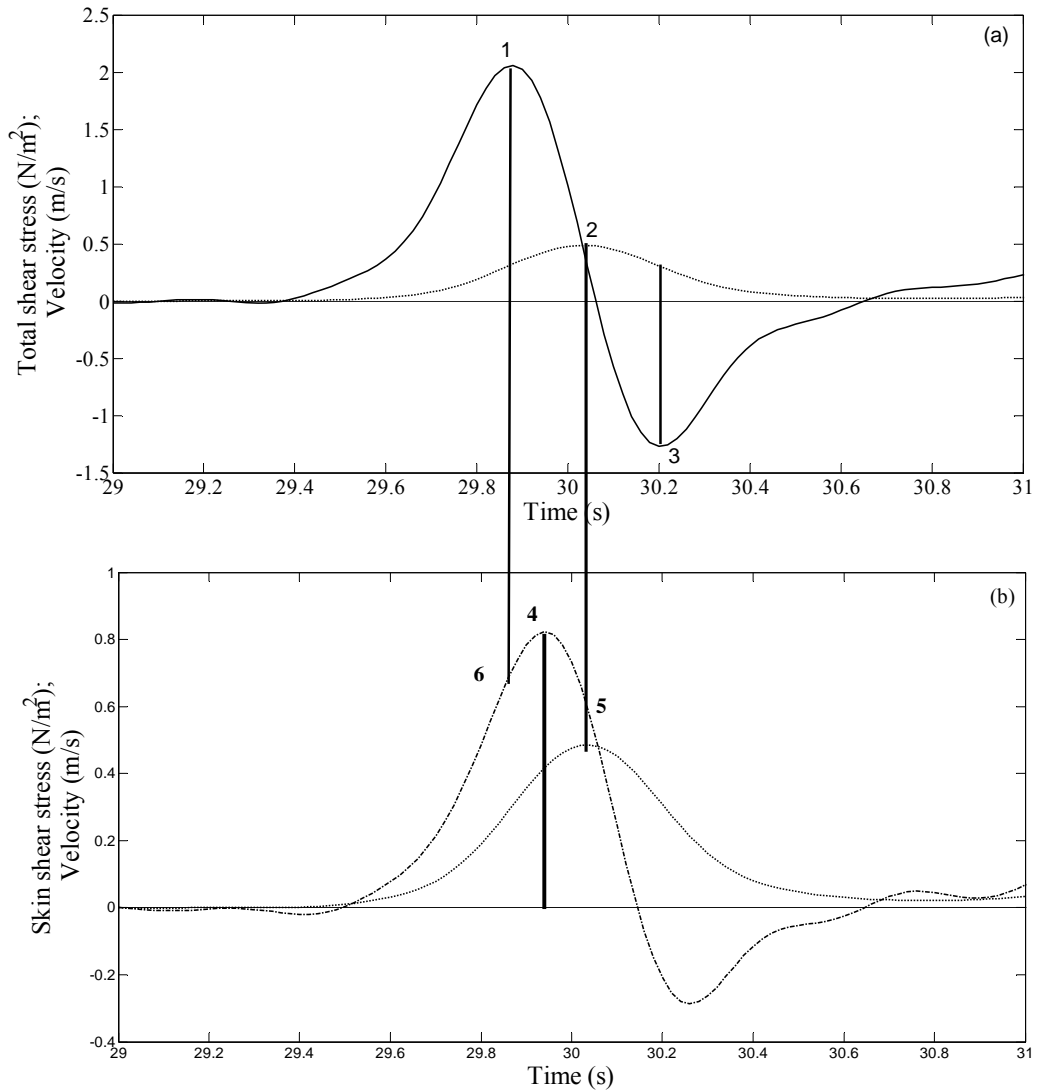


Fig. 8. Typical measured parameters. (a) _____ Total shear stress; velocity; Point 1 corresponds to maximum measured total shear stress; Point 2 corresponds to total shear stress at time of maximum velocity; Point 3 corresponds to minimum total shear (b) estimated skin shear stress; velocity. Point 4 corresponds to maximum skin shear stress; Point 5 corresponds to skin shear stress at time of maximum velocity; Point 6 corresponds to skin shear at time of maximum total shear.

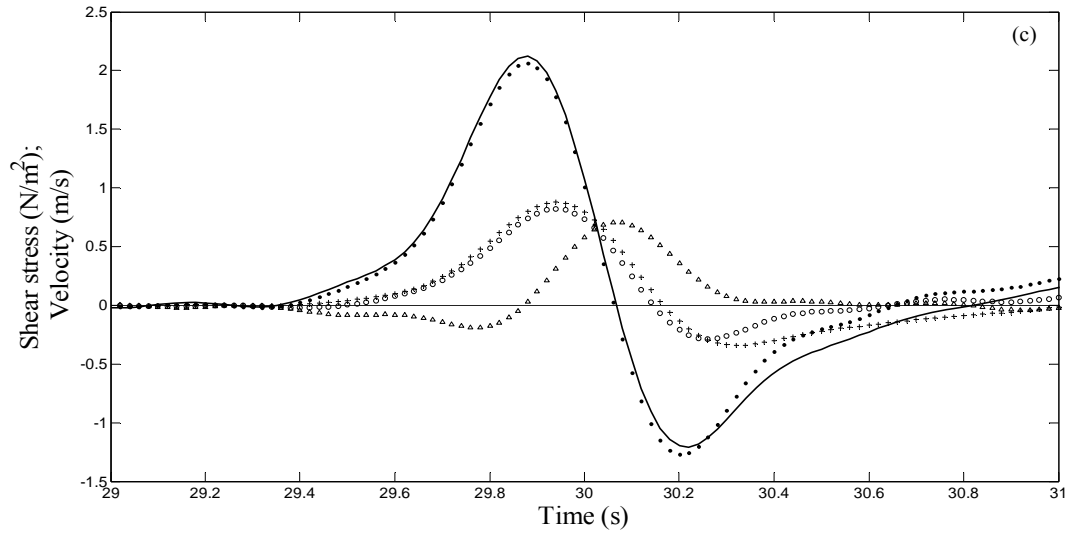


Fig. 8c. Comparison of measured Total shear stress and skin shear stress with laminar theory of Liu (2007). Solid line – predicted total shear stress; dots – measured total shear stress; circles – estimated skin shear stress for 65% pressure gradient force; crosses – predicted skin shear stress from measured velocity as per Liu (2007); triangles – measured skin shear stress for 100% pressure gradient force.

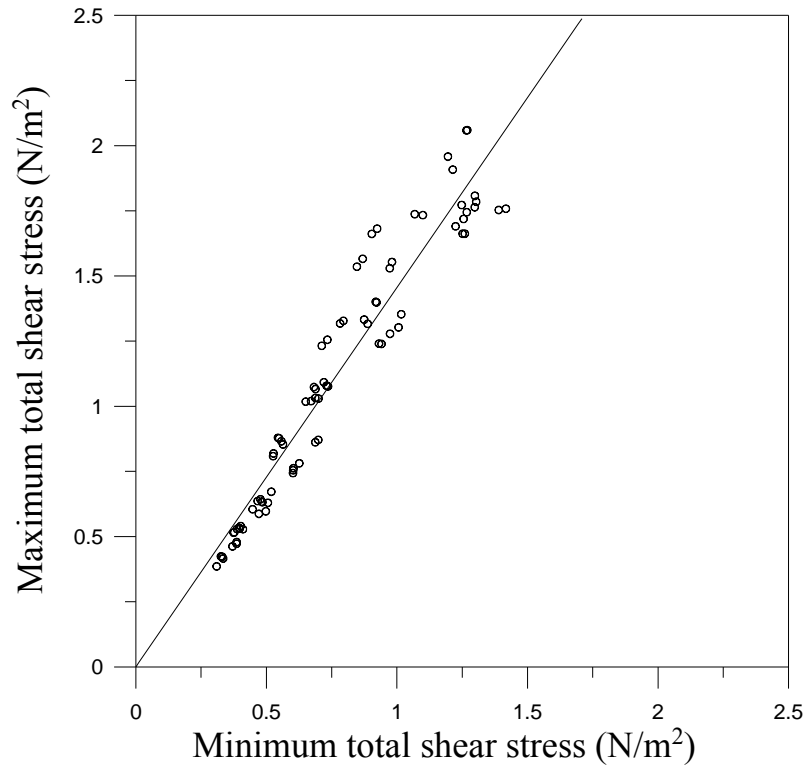


Fig. 9. Comparison between measured maximum and minimum τ_T . ($\tau_{T,\max} = 1.46\tau_{T,\min}$; $R^2 = 0.987$).

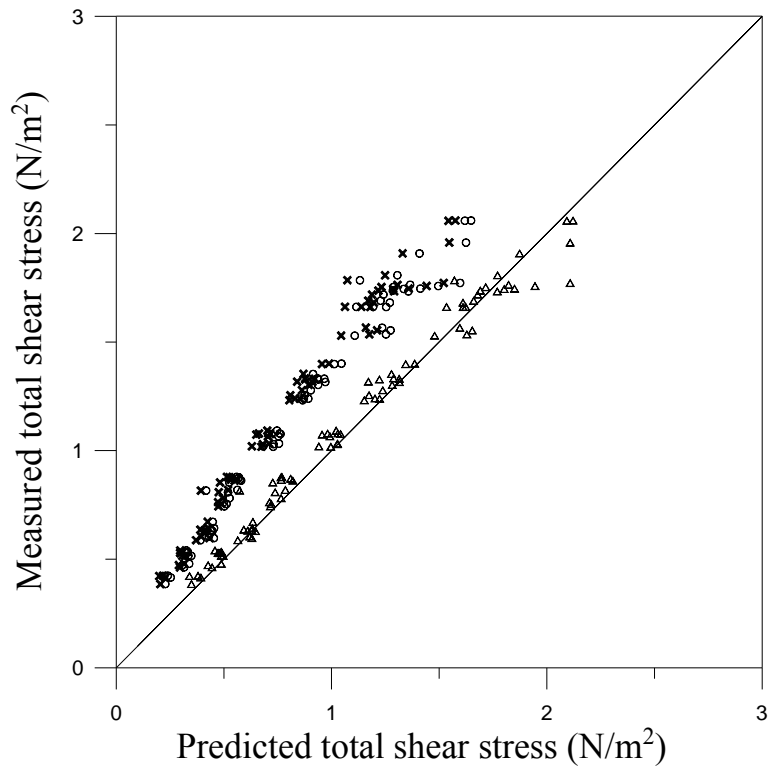


Fig. 10. Comparison between measured and predicted total shear stress from convolution methods. Triangles $q=1/2$ in Eq.16 and $\nu_e =$ kinematic viscosity (laminar solution); Circles $q=1/8$ and ν_e from Eq.17; Crosses $q = 1/8$ and ν_e from Eq.18.

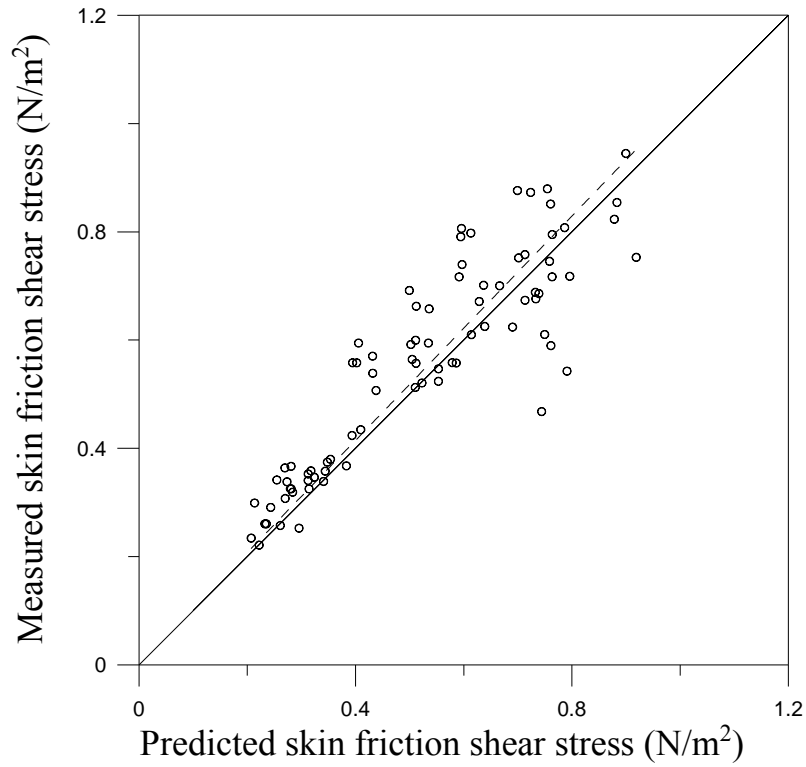


Fig. 11. Comparison between measured and predicted skin friction shear stress from convolution method. Circles $q = 1/2$ in Eq.16 and $\nu_e =$ kinematic viscosity; - - - - best fit line; ($\tau_m = 1.04\tau_p$; $R^2 = 0.974$).

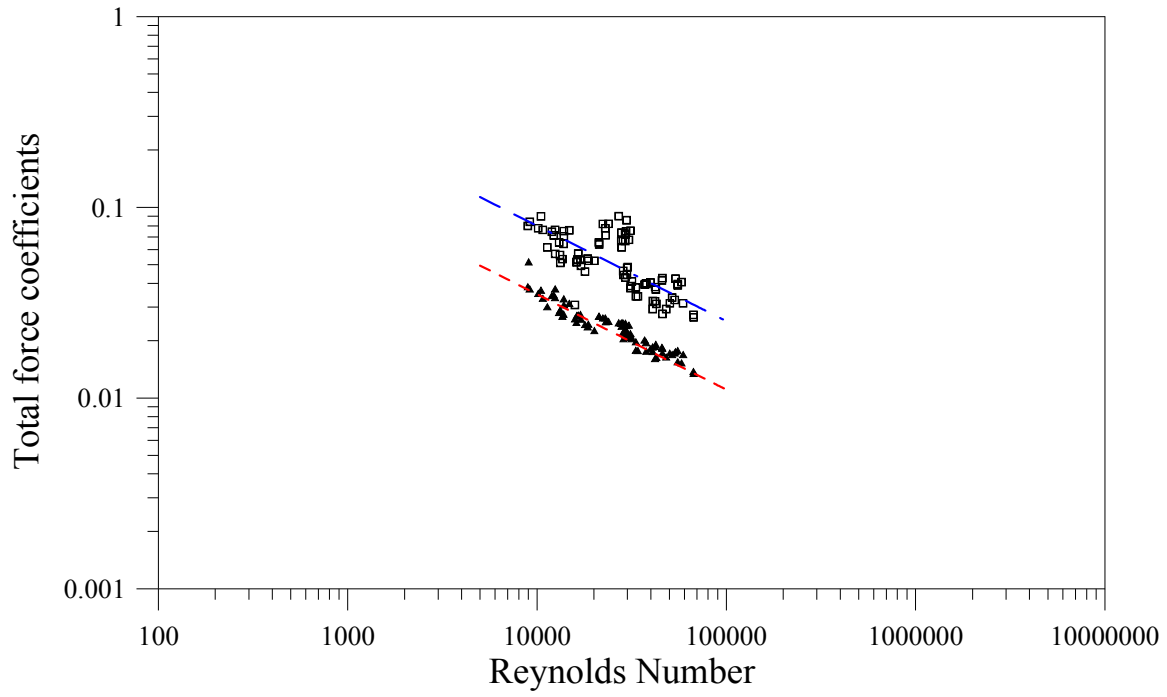


Fig. 12. Total shear stress coefficients at maximum τ_T (Point-1, Fig. 8) estimated from Eq.21. Triangles correspond to the coefficients estimated using u_{\max} ; Squares correspond to coefficients estimated using instantaneous velocity. (- - - corresponds to $f_T = 3.5/\sqrt{R_e}$; - . - . - corresponds to $f_T = 8/\sqrt{R_e}$).

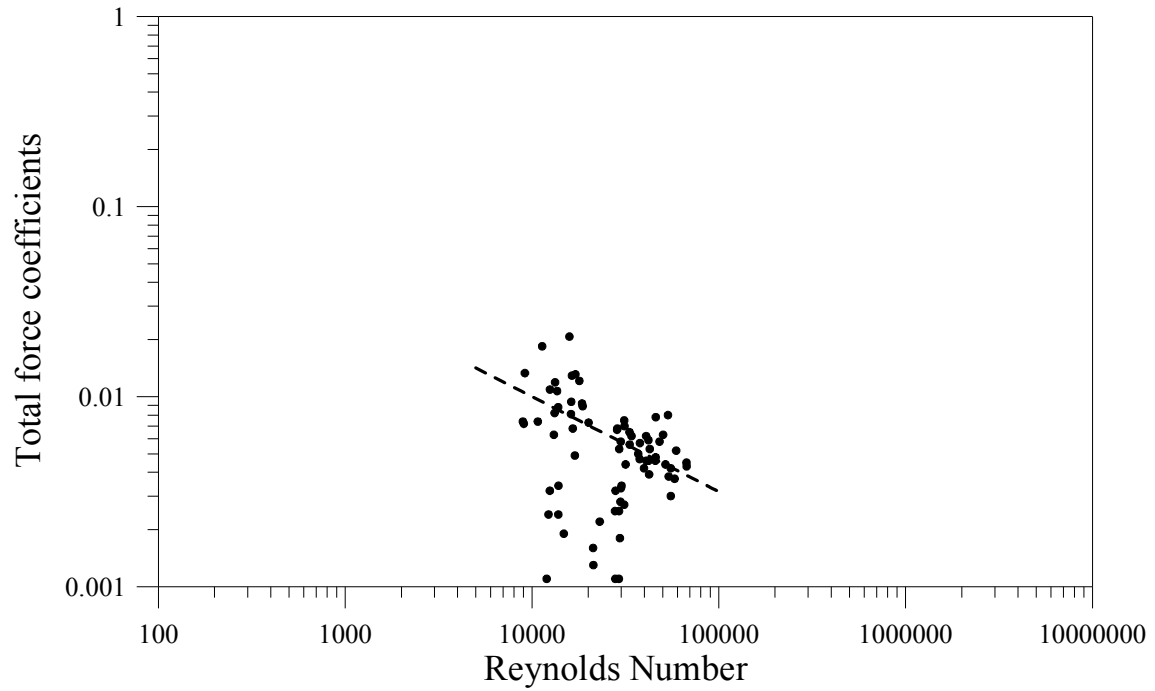


Fig. 13. Total shear stress coefficients at u_{\max} (Point-2, Fig. 8) estimated from Eq.21; (- - - corresponds to $f_T = 1/\sqrt{R_e}$).

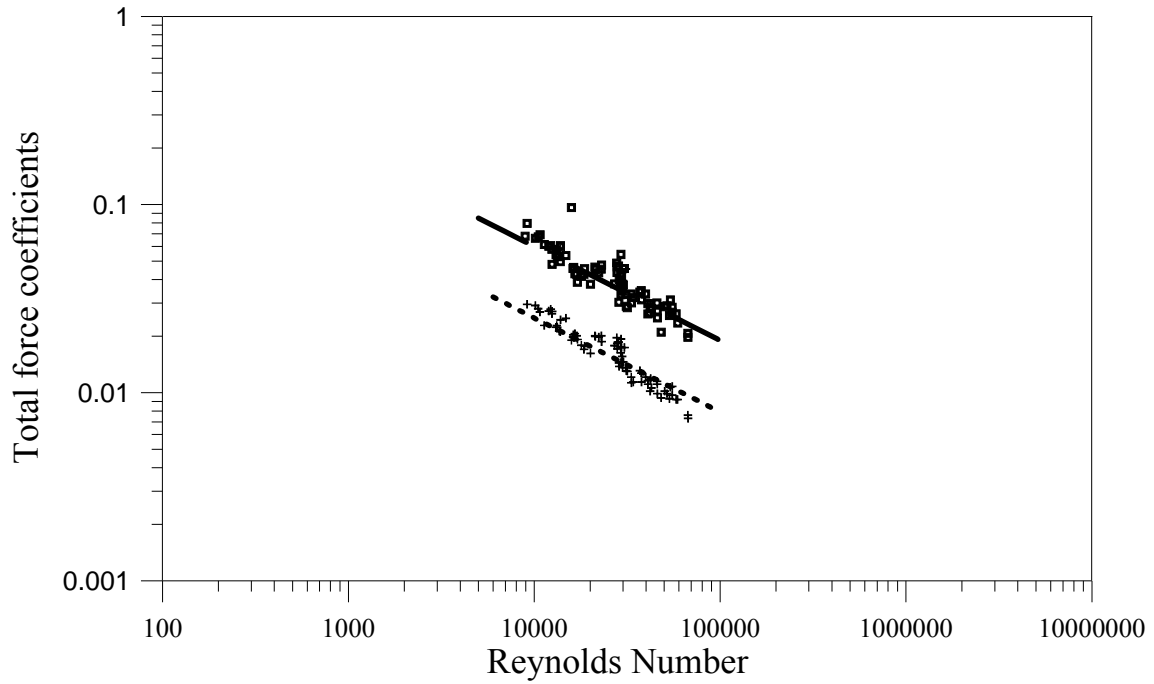


Fig. 14. Total shear stress coefficients at minimum τ_T (Point-3, Fig. 8) estimated from Eq.21. Crosses correspond to the coefficients estimated using u_{\max} . Squares correspond to coefficients estimated using velocity corresponding to minimum τ_T . (---- corresponds to $f_T = 2.5/\sqrt{R_e}$; - . - . - corresponds to $f_T = 6/\sqrt{R_e}$).

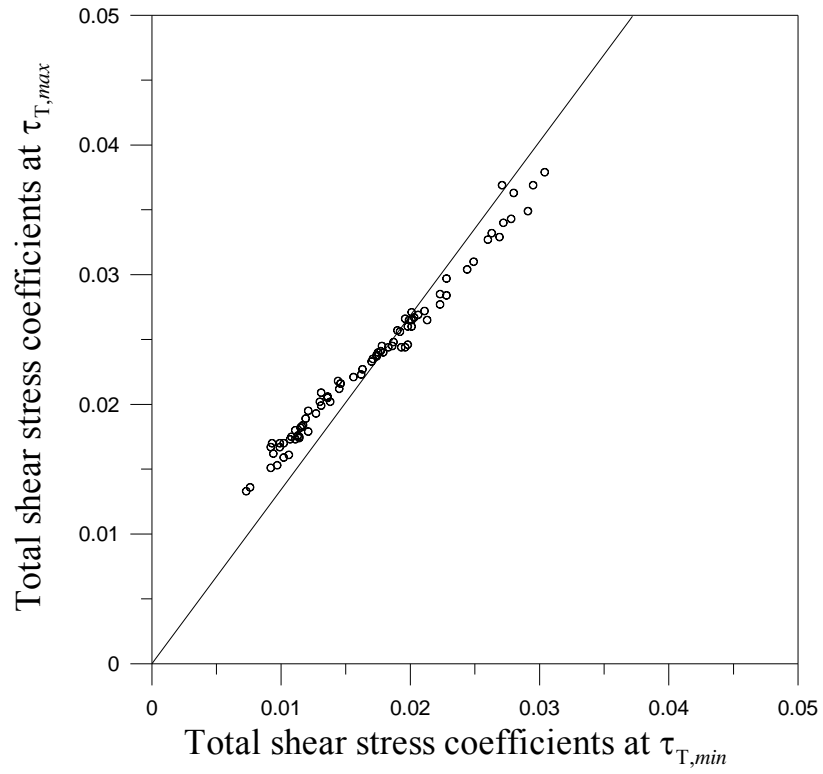


Fig. 15. Total shear stress coefficients at $\tau_{T,max}$ and $\tau_{T,min}$ (Points 1 and 3 in Fig. 8) estimated using u_{max} . ($\tau_{T,max} = 1.34\tau_{T,min}$; $R^2 = 0.991$).

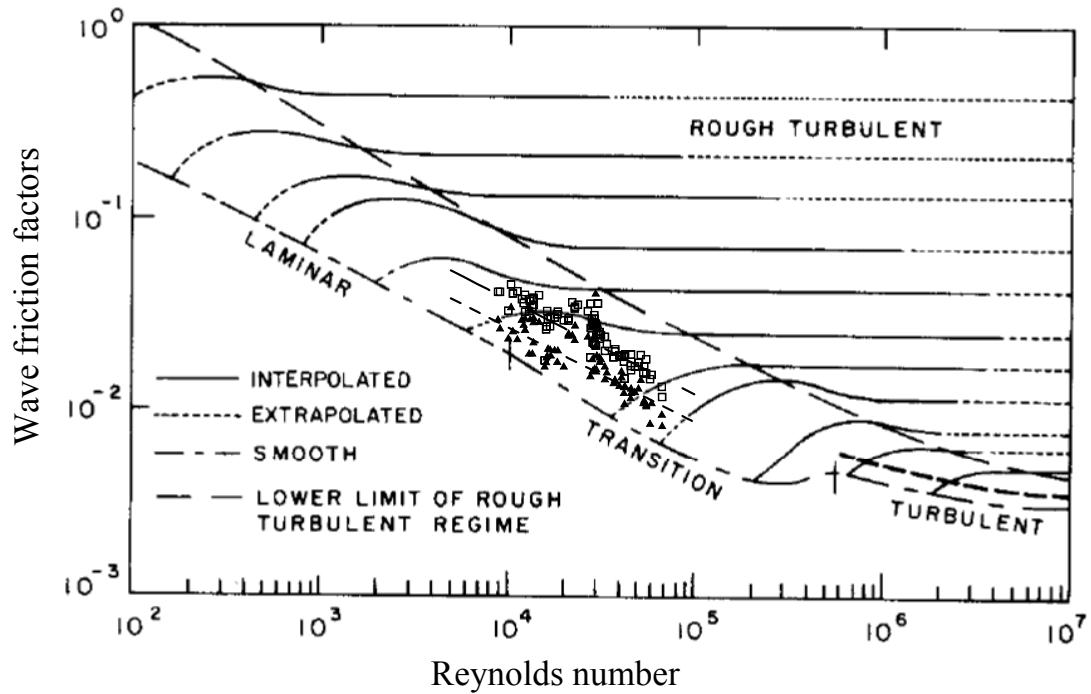


Fig. 16. Wave friction factors at maximum τ (Point-4, Fig. 8) estimated from Eq.21 plotted on wave friction factor diagram of Kamphuis (1975). Triangles correspond to the friction factors estimated using maximum velocity. Squares correspond to friction factors estimated using velocity corresponding to maximum shear stress. (- - - corresponds to $f = 2.5/\sqrt{R_e}$; - - - - corresponds to $f = 3.5/\sqrt{R_e}$).

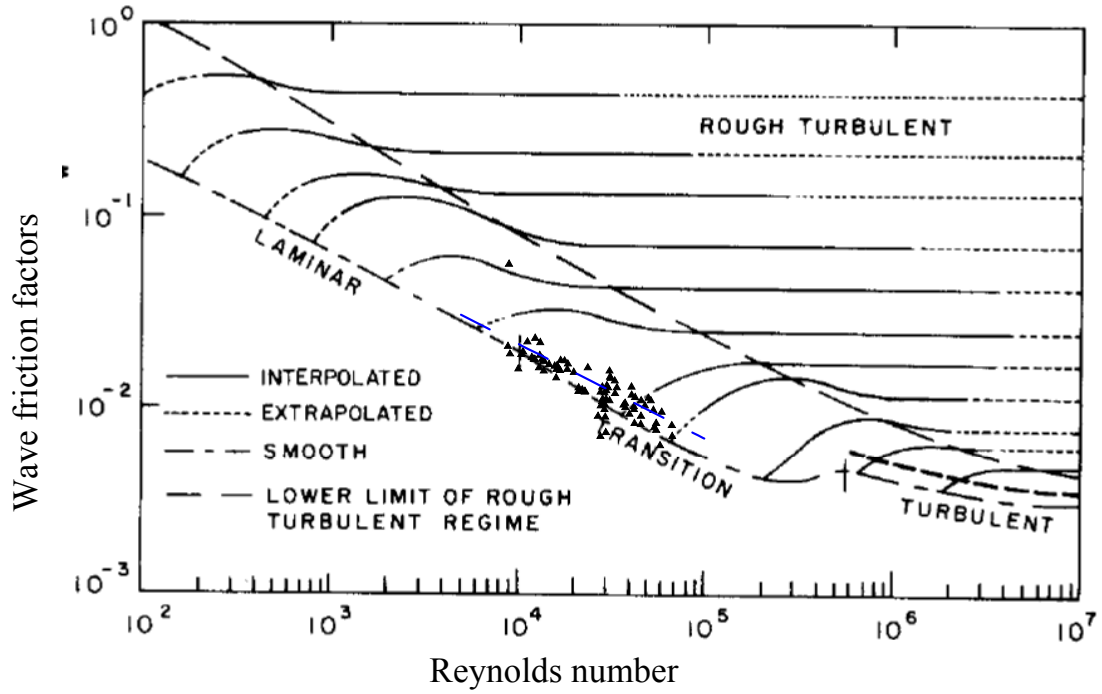


Fig. 17. Wave friction factors at u_{max} (Point-5, Fig. 8) estimated from Eq.21 plotted on wave friction factor diagram of Kamphuis (1975). (- - - - corresponds to $f = 2/\sqrt{R_c}$).

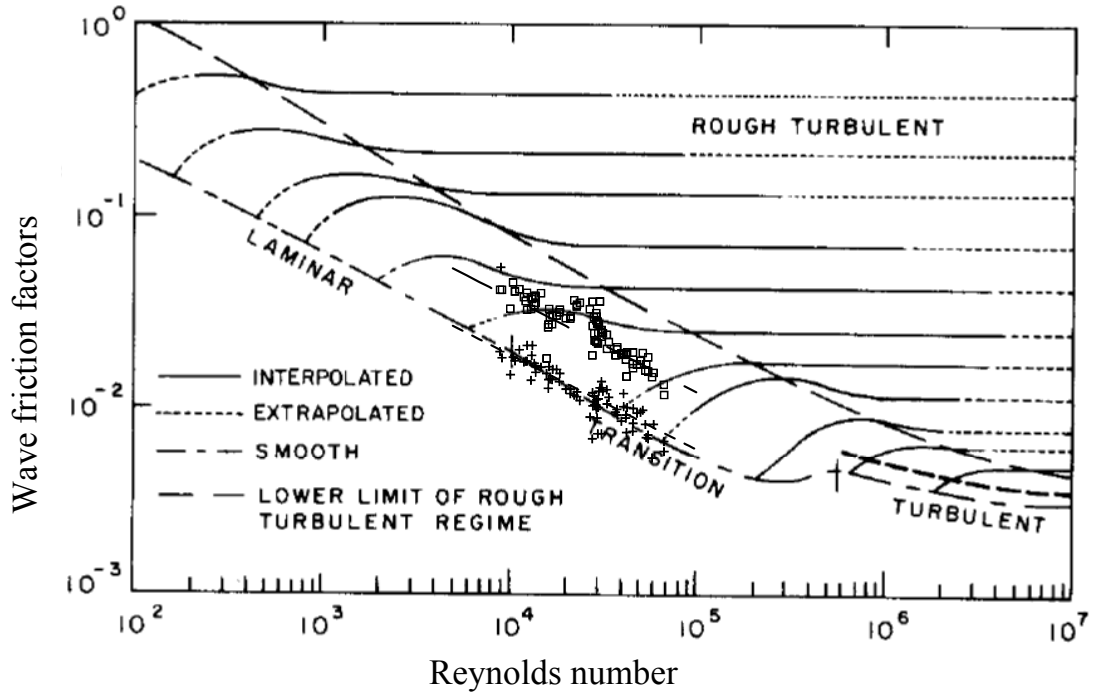


Fig. 18. Wave friction factors at time of maximum τ_T (Point-6, Fig. 8) estimated from Eq.21 plotted on wave friction factor diagram of Kamphuis (1975). ++++ correspond to the coefficients estimated using maximum velocity. Squares correspond to coefficients estimated using instantaneous velocity. (- - - - corresponds to $f = 1.75/\sqrt{R_e}$; - - - - corresponds to $f = 3.5/\sqrt{R_e}$).

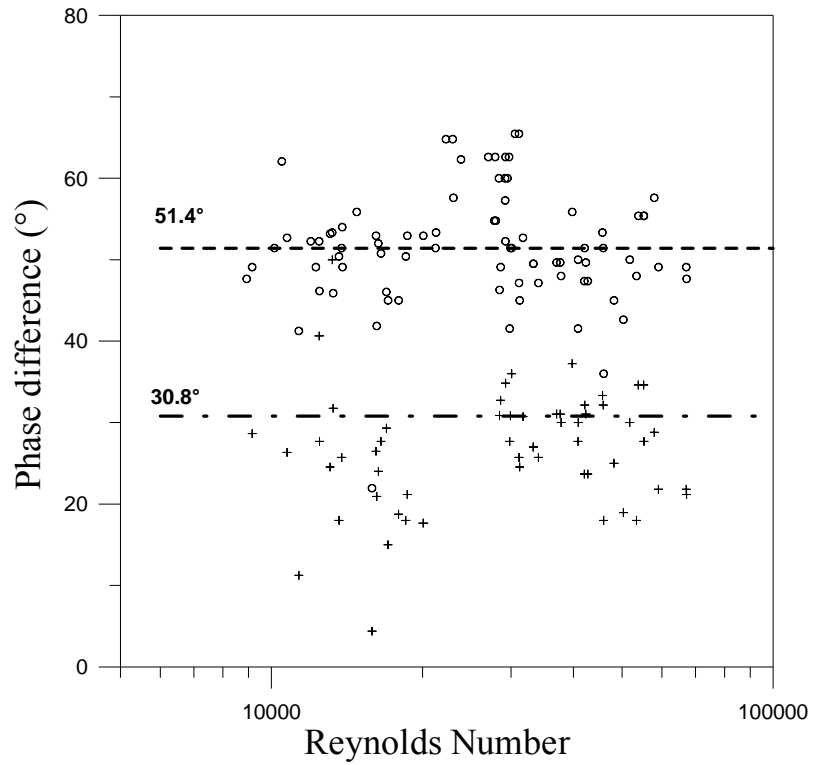


Fig. 19. Measured phase differences between u_{\max} and $\tau_{T,\max}$ (Point 2 and Point 1 of Fig. 8) (oooo median 51.4°), and u_{\max} and τ_{\max} (point 2 and point 4 of Fig. 8) (++++ median 30.85°)

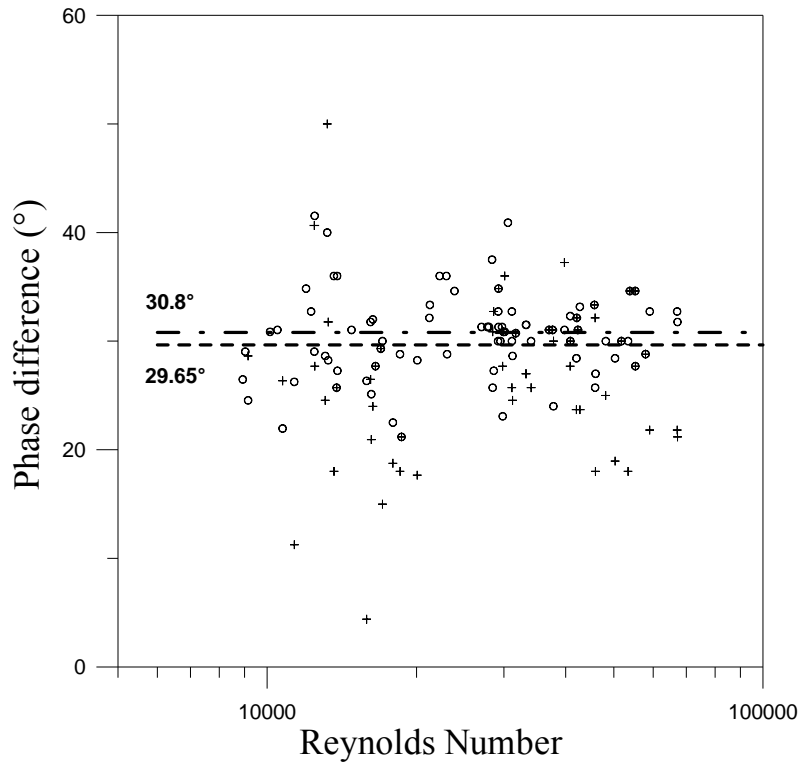


Fig. 20. Phase differences between u_{\max} and measured τ_{\max} (point 2 and point 4 of Fig. 8) (+++ median 30.8°) and u_{\max} and predicted τ_{\max} estimated using Eqs. 10 and 16 (ooo median 29.65°)